A lipodystrophy-causing lamin A mutant alters conformation and epigenetic regulation of the anti-adipogenic *MIR335* locus

Anja Oldenburg,[1] Nolwenn Briand,[1] Anita L. Sørensen,[1] Inswasti Cahyani,[1] Akshay Shah,[1] Jan Øivind Moskaug,[1,2] and Philippe Collas[1,2]

[1]Department of Molecular Medicine, Institute of Basic Medical Sciences, Faculty of Medicine, University of Oslo, Oslo, Norway
[2]Norwegian Center for Stem Cell Research, Department of Immunology, Oslo University Hospital, Oslo, Norway

Mutations in the *Lamin A/C* (*LMNA*) gene-encoding nuclear LMNA cause laminopathies, which include partial lipodystrophies associated with metabolic syndromes. The lipodystrophy-associated LMNA p.R482W mutation is known to impair adipogenic differentiation, but the mechanisms involved are unclear. We show in this study that the lamin A p.R482W hot spot mutation prevents adipogenic gene expression by epigenetically deregulating long-range enhancers of the anti-adipogenic *MIR335* microRNA gene in human adipocyte progenitor cells. The R482W mutation results in a loss of function of differentiation-dependent lamin A binding to the *MIR335* locus. This impairs H3K27 methylation and instead favors H3K27 acetylation on *MIR335* enhancers. The lamin A mutation further promotes spatial clustering of *MIR335* enhancer and promoter elements along with overexpression of the *MIR355* gene after adipogenic induction. Our results link a laminopathy-causing lamin A mutation to an unsuspected deregulation of chromatin states and spatial conformation of an miRNA locus critical for adipose progenitor cell fate.

Introduction

The nuclear lamina is a meshwork of A- and B-type lamins at the nuclear envelope and contributes to the spatial organization of chromatin and regulation of gene expression. Although lamins B1 and B2 are mostly restricted to the nuclear lamina at the nuclear periphery, lamin A/C (LMNA) is found both at the nuclear periphery and in the nuclear interior. There, LMNA can also interact with chromatin (Lund et al., 2013, 2015; Gesson et al., 2016), and in doing so, it is able to modulate somatic stem cell differentiation (Naetar and Foisner, 2009). Mutations throughout the *LMNA* gene cause various forms of laminopathies, including partial lipodystrophies (Vigouroux et al., 2011). The heterozygous LMNA p.R482W mutation is the most frequent mutation causing familial partial Dunnigan lipodystrophy (FPLD2; OMIM ID, 151660), characterized by a redistribution of adipose tissue, general muscle hypertrophy, and metabolic disorders (Decaudain et al., 2007; Vigouroux et al., 2011). How the hot spot LMNA p.R482W mutation causes FPLD2 probably involves a deregulation of signaling pathways (Le Dour et al., 2017), of nucleus and cell mechanosensitivity (Osmanagic-Myers et al., 2015), and of nuclear architecture (Vigouroux et al., 2001). Studies in mice, patient cells, and cultured preadipocytes concur in that the mutation leads to adipogenic differenti-

ation defects (Boguslavsky et al., 2006; Oldenburg et al., 2014; Vadrot et al., 2015). Moreover, the R482W mutation impairs LMNA interaction with the adipogenic factor SREBP1 (Vadrot et al., 2015) and with DNA in vitro (Stierlé et al., 2003). These findings are supported by recent work showing that although the majority of chromatin domains (so-called lamin-associated domains; LADs) interacting with LMNA are conserved between fibroblasts of healthy and FPLD2 patients, some are variable (Paulsen et al., 2017). These observations suggest a differential regulatory influence of WT and mutant LMNA on chromatin organization.

We have earlier identified fragile X–related protein 1 (FXR1P), a promyogenic protein (Huot et al., 2005; van't Padje et al., 2009; Davidovic et al., 2013), as a binding partner of LMNA, whose association with LMNA is weakened by the LMNA(R482W) mutation (Oldenburg et al., 2014). Expression of the R482W mutation in human primary adipose stem cells (ASCs) up-regulates FXR1P levels and elicits myogenic gene expression (Oldenburg et al., 2014). FXR1P up-regulation, however, does not result from an increase in *FXR1* mRNA levels, suggesting a posttranscriptional or posttranslational deregulation.

Correspondence to Philippe Collas: philc@medisin.uio.no

Abbreviations used: 335-i, miR-335 inhibitor; 335-m, miR-335 mimic; ASC, adipose stem cell; ChIP, chromatin immunoprecipitation; EDMD, Emery-Dreifuss muscle dystrophy; LAD, lamin-associated domain; LMNA, lamin A/C; MSC, mesenchymal stem cell; qPCR, quantitative PCR; TSS, transcription start site.
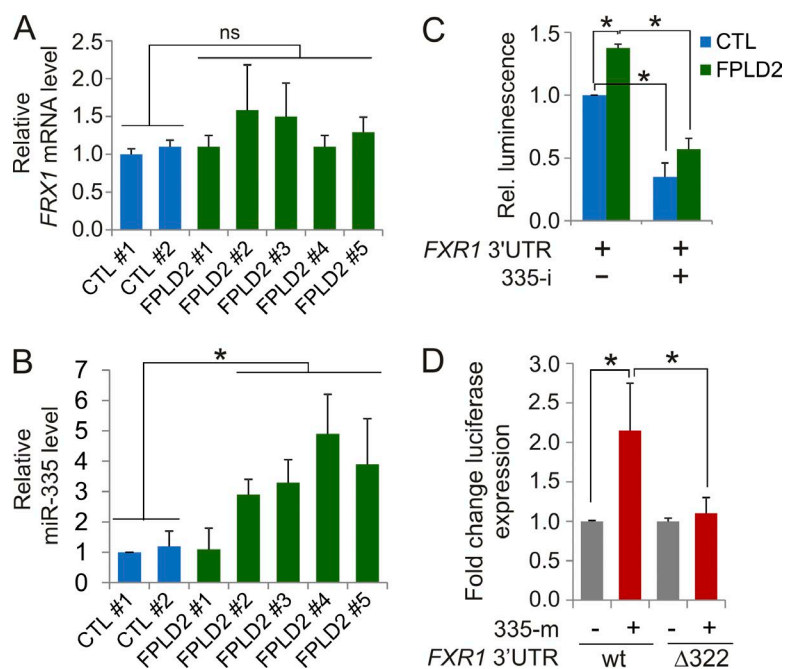
Figure 1. **FXR1P protein level in FPLD2 patient fibroblasts is regulated by miR-335.** (A) RT-qPCR analysis of *FXR1* mRNA in control (CTL) and FPLD2 fibroblasts (patients 1–5; ^{ns}P > 0.01; ANOVA; means ± SD of a triplicate analysis). (B) RT-qPCR analysis of miR-335 levels in control and FPLD2 fibroblasts (*, P = 0.002; ANOVA; means ± SD of a triplicate analysis). (C) Luciferase activity from a reporter upstream of the *FXR1* 3′ UTR in control and FPLD2 fibroblasts treated with 0 or 500 nM 335-i (*, P < 0.01; Fisher's exact test; means ± SD of a triplicate experiment). (D) miR-335 targets the 3′ UTR of the *FXR1* mRNA. A WT or mutated luciferase-*FXR1* 3′ UTR reporter was expressed in DT40 cells after DICER knockdown; the mutation was a deletion of the predicted miR-335 binding site at position −322 (Δ322). Luciferase activity was measured 24 h after introduction of 0 or 500 nM 335-m (*, P < 0.01; Fisher's exact test; means ± SD of a triplicate experiment).

One mechanism of *FXR1* deregulation may involve miRNAs (Cheever et al., 2010). miRNAs are short, noncoding RNAs that commonly down-regulate target mRNAs through degradation or translational silencing after binding to the 3′ UTR. Interestingly, however, some miRNAs can stabilize mRNAs and promote translational activation (Vasudevan et al., 2007). Because single miRNAs often target multiple transcripts, they can be involved in many normal and pathological processes including lipid metabolism (Fernández-Hernando et al., 2011), mesenchymal stem cell (MSC) differentiation (Tomé et al., 2011), and diseases including cancer (Small and Olson, 2011; Lujambio and Lowe, 2012).

Interestingly, miRNAs including miR-335 have been shown to be deregulated in muscle biopsies of patients with LMNA-linked muscle dystrophy (Sylvius et al., 2011). miR-335 is promyogenic (Meyer et al., 2015), inhibits MSC differentiation into adipocytes and osteocytes (Tomé et al., 2011), and is involved in mesendodermal and chondrogenic induction (Lin et al., 2014; Yang et al., 2014). This attests to a role of miR-335 in the differentiation fate of MSCs. miR-335 is up-regulated in obese adipose tissue (Oger et al., 2014) and in senescent MSCs (Tomé et al., 2014). It is also implicated in adipose tissue inflammation (Zhu et al., 2014) and in transcriptional deregulation in type-2 diabetes patients (Calimlioglu et al., 2015). Strikingly, all these features are hallmarks of FLPD2 (Vigouroux et al., 2011). Nevertheless, miR-335 has to date not been implicated in lipodystrophic laminopathies. We show in this study that the lipodystrophic LMNA p.R482W mutation prevents adipogenic gene expression via up-regulation of miR-335 in a process involving epigenetic and conformational alterations of the *MIR335* locus.

Results

FXR1P level is deregulated via miR-335 in FPLD2 patient fibroblasts

Fibroblasts from FLPD2 patients with the LMNA p.R482W mutation harbor elevated FXR1P protein levels with no significant variations in *FXR1* transcripts compared with WT fibroblasts (Oldenburg et al., 2014). We now extend these observations to fibroblasts from additional FPLD2 patients with the same LMNA mutation (Figs. 1 A and S1 A). Treatment of WT fibroblasts with the proteasome inhibitor MG132 did not enhance FXR1P levels, but as expected, they elevated P53 levels (Fig. S1 B), suggesting that elevated FXR1P in FPLD2 fibroblasts does not result from reduced protein degradation by the proteasome.

Rather, this could involve posttranscriptional processing of *FXR1* transcripts by miRNAs (Cheever and Ceman, 2009). One miRNA up-regulated in LMNA-linked myodystrophy is the promyogenic miR-335 (Sylvius et al., 2011). miR-335 is also anti-adipogenic (Tomé et al., 2011) and predicted to target the 3′ UTR of *FXR1* (Fig. S1 C). Given the lipodystrophy and muscle hypertrophy symptoms of FPLD2 patients, we examined miR-335 levels in control and FPLD2 fibroblasts. Strikingly, TaqMan reverse-transcription quantitative PCR (qPCR) revealed significant overall up-regulation of miR-335 in FPLD2 fibroblast cultures (P = 0.002; ANOVA; Fig. 1 B). The *MIR335* gene lies within intron 2 of the *MEST* gene on chromosome 7q21.11. *MIR335* and *MEST* have been shown to be coregulated in cancer (Png et al., 2011; Hiramuki et al., 2015) but not in cases of adipose tissue inflammation (Zhu et al., 2014). However, *MEST* mRNA levels remain low in control and FPLD2 fibroblasts (Fig. S1 D), indicating that *MIR335* and *MEST* are not coregulated under these conditions. The repressed state of *MEST* was supported by high CpG methylation in the locus in both cell types (Fig. S1 E). Thus, *MIR335* is up-regulated independently of expression of its host gene *MEST* in FPLD2 patient fibroblasts.

Up-regulation of both FXR1P and miR-335 in FPLD2 fibroblasts suggests that miR-335 positively influences FXR1P protein level in these cells. To test this, we transfected control and FPLD2 fibroblasts with a luciferase reporter cloned upstream of the 3′ UTR of the *FXR1* mRNA and asked whether miR-335 was able to up-regulate luciferase expression. Indeed, luciferase activity was increased in FPLD2 cells in correlation with elevated miR-335 levels (P < 0.01; Fisher's exact test;
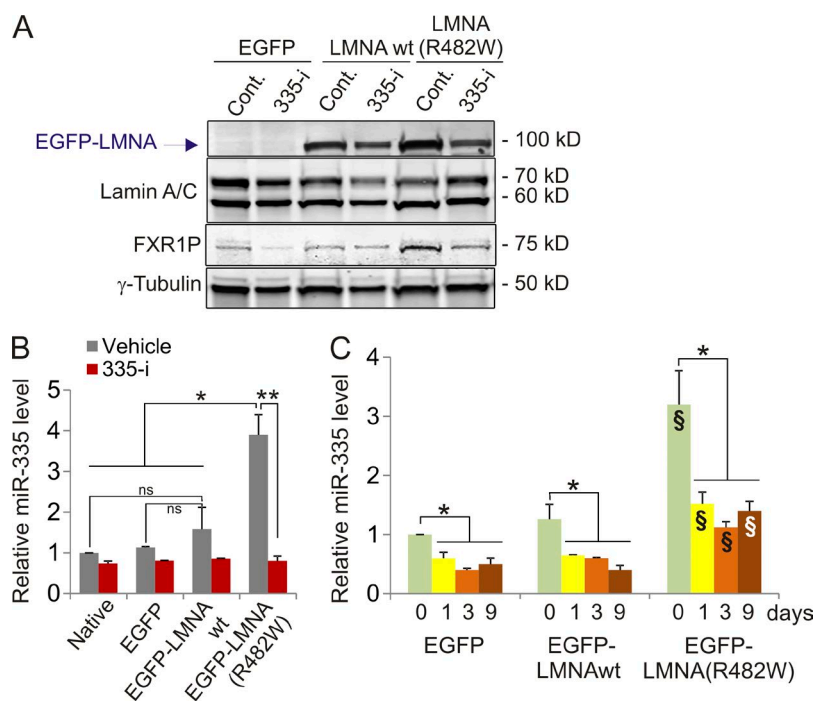
Figure 2. Expression of LMNA(R482W) in ASCs up-regulates miR-335 expression. (A) Western blot analysis of EGFP-LMNA (anti-EGFP antibodies), endogenous LMNA, and FXR1P in ASC^{EGFP}, ASC^{LMNAWT}, and ASC$^{LMNA(R482W)}$. γ-Tubulin was used as a loading control. (B) Relative miR-335 levels in native ASCs, ASC^{EGFP}, ASC^{LMNAWT}, and ASC$^{LMNA(R482W)}$ treated with 500 nM 335-i or a vehicle control (*, $P = 0.001$; ANOVA; **, $P < 0.001$; Fisher's exact test; $^{ns}P > 0.05$; post-ANOVA Fisher's exact test; means ± SD of triplicate transfections and analyses). (C) Relative miR-335 levels in ASC^{EGFP}, ASC^{LMNAWT}, or ASC$^{LMNA(R482W)}$ differentiated for up to 9 d (*, $P < 0.001$; ANOVA; $^{§}P < 0.001$; ANOVA for the same time points in ASC^{EGFP} and ASC^{LMNAWT} control cells; means ± SD of a triplicate differentiation).

Fig. 1 C). Cotransfection of a specific hairpin miR-335 inhibitor (335-i; 500 nM), however, significantly reduced luciferase activity ($P < 0.01$; Fisher's exact test; Fig. 1 C), suggesting that miR-335 positively regulates *FXR1* mRNA translation. Because some miRNAs can positively regulate their target mRNAs (Vasudevan et al., 2007; Cheever and Ceman, 2009), we then tested whether miR-335 was able to target *FXR1* transcripts. To abrogate any effect of endogenous miR-335 or of any miRNA that would target *FXR1*, we transfected the luciferase-*FXR1* 3′ UTR reporter construct in DT40 cells depleted of the RNA interference machinery by inducible knockdown of DICER (Fig. S1 F; Fukagawa et al., 2004). This would enable the luciferase-*FXR1* 3′ UTR reporter to be regulated by an exogenously added miRNA. Cotransfection of a miR-335 mimic (335-m) oligonucleotide (5 μM) led to luciferase up-regulation, and deletion of the predicted miR-335 target site at position 322 in the *FXR1* 3′ UTR abolishes this up-regulation ($P < 0.01$; Fisher's exact test; Fig. 1 D). Thus miR-335 was able to up-regulate the *FXR1* mRNA by targeting its 3′ UTR. This implicates miR-335 in the up-regulation of FXR1P linked to expression of LMNA(R482W) in FPLD2 patient cells.

The LMNA(R482W) mutation up-regulates miR-335 levels in primary ASCs

We next assessed whether, as in fibroblasts, miR-335 was up-regulated in human ASCs expressing LMNA(R482W) (hereafter called ASC$^{LMNA(R482W)}$). Expression of EGFP-LMNA(R482W) but not EGFP-LMNA WT or EGFP alone (Fig. 2 A) significantly up-regulated miR-335 ($P = 0.001$; ANOVA; Fig. 2 B). This up-regulation was specific because it was blocked with 500 nM 335-i ($P < 0.001$; Fisher's exact test; Fig. 2 B). FXR1P was also up-regulated in ASC^{LMNAWT} and ASC$^{LMNA(R482W)}$ in a manner sensitive to miR335 inhibition ($P < 0.01$; Fisher's exact test; Figs. 2 A and S1 G). This directly implicates miR-335 in the up-regulation of FXR1P elicited by LMNA(R482W) not only in fibroblasts but also in ASCs. Because both miR-335 and FXR1P have promyogenic properties, these results are consistent with the induction of myogenic gene and protein expression previously shown in ASC$^{LMNA(R482W)}$ (Oldenburg et al., 2014). These data also show the relevance of miR-335 and FXR1P overexpression to the muscle hypertrophy phenotype characteristic of FPLD2 patients (Decaudain et al., 2007).

Induction of adipogenic differentiation substantially decreased miR-335 levels in ASC$^{LMNA(R482W)}$ ($P < 0.001$; ANOVA; Fig. 2 C). miR-335 down-regulation also occurred in differentiating ASC^{LMNAWT} and control ASC^{EGFP} ($P < 0.001$; ANOVA; Fig. 2 C), consistent with the anti-adipogenic property of miR-335 (Tomé et al., 2011). Strikingly, however, in ASC$^{LMNA(R482W)}$, miR-335 remained higher than in controls at each stage of differentiation, even after 9 d ($^{§}P < 0.001$; ANOVA; Fig. 2 C). These miR-335 levels were similar to those of undifferentiated native ASCs, suggesting that they may be inhibitory to adipogenic differentiation. Interestingly, expression of the Emery-Dreifuss muscle dystrophy (EDMD)-causing LMNA(R453W) mutant in ASCs also elicited up-regulation of miR-335 in undifferentiated cells; importantly, however, unlike R482W, the R453W mutation was compatible with a marked return of miR-335 to basal levels on day 9 of differentiation as in cells expressing WT LMNA (Fig. S2 A). Thus, among the LMNA constructs examined in this study, maintenance of elevated miR-335 levels after adipogenic induction was specific for the lipodystrophic R482W mutation. Our results also suggest that elevated miR-335 levels in undifferentiated cells do not compromise adipose cell fate, but down-regulation of miR-335 is essential for differentiation to occur.

miR-335 inhibition rescues deficiencies in adipogenic gene expression elicited by LMNA(R482W) expression

We previously reported that expression of LMNA(R482W) in ASCs impairs adipogenic differentiation (Oldenburg et al., 2014); we confirm this observation in this study by showing decreased expression of perilipin, a marker of lipid droplets, in in-cell Western assays (Fig. S2 B). Because ASC$^{LMNA(R482W)}$
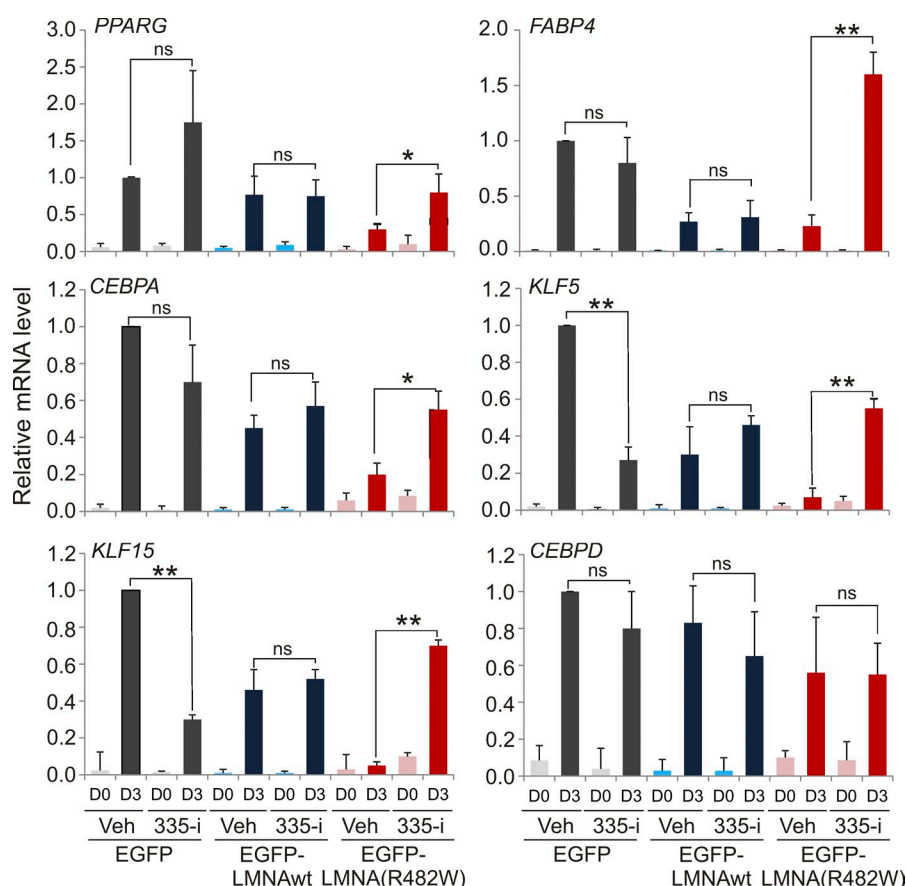
Figure 3. **miR-335 inhibition restores adipogenic gene expression inhibited in ASCs by the LMNA(R482W) mutation.** RT-qPCR analysis of indicated transcripts in ASCs on day 0 (D0) and day 3 (D3) of adipogenic differentiation treated with vehicle (Veh) or 500 nM 335-i (*, P < 0.01; **, P < 0.001; Fisher's exact tests; means ± SD of triplicate differentiations).

overexpresses miR-335, we determined whether restoring miR-335 to background levels would rescue adipogenic gene expression in these cells. Expression of LMNA(R482W) in ASCs impaired expression of adipocyte transcripts including *PPARG*, *CEBPA*, *FABP4*, *KLF5*, and *KLF15* (the latter two being *PPARG* activators) after adipogenic induction (Fig. 3). LMNA WT also reduced expression of some of these transcripts in line with other studies also reporting adverse effects of overexpressing WT LMNA (Favreau et al., 2004; Scaffidi and Misteli, 2008; Oldenburg et al., 2014; Vadrot et al., 2015; Lee et al., 2016). Moreover, 335-i abrogated miR-335 elevation invoked by LMNA(R482W) (P < 0.01; Fisher's exact test; Fig. 2 B) and thus could be used in a rescue experiment. Strikingly, we found that 335-i restored expression of all adipogenic transcripts inhibited in ASC[LMNA(R482W)] (day 3; P < 0.01; Fisher's exact test; Fig. 3). *CEPBA*, *CEPBD*, *FABP4*, *KLF5*, or *KLF15* are predicted targets of miR-335, making a direct effect of miR-335 on these transcripts unlikely. However, the 3′ UTR of *PPARG* is a predicted miR-335 target, so miR-335 inhibition could affect expression of the PPARγ transcription factor and of its targets. In ASC[LMNAWT], the effect of miR-335 inhibition on transcripts that are also down-regulated is minimal (e.g., *FABP4*, *CEBPA*, *KLF5*, and *KLF15*); however, in these cells, mRNA levels do not significantly differ from those of control ASC[EGFP] treated with 335-i (Fig. 3). We conclude that miR-335 inhibition relieves the impairment of adipogenic gene expression elicited by the lipodystrophic LMNA(R482W) mutation. Thus, one mechanism by which the R482W mutation impairs adipogenic induction is by maintaining high levels of anti-adipogenic miR-335.

LMNA exerts a repressive role on the MIR335 locus during adipogenic differentiation

We next investigated the mechanisms by which LMNA could regulate *MIR335* gene expression in ASCs. LMNA interacts with chromatin mostly in transcriptionally inactive regions, providing one potential level of gene regulation. The *MEST* gene, which hosts *MIR335*, is located ~400 kb downstream of the nearest LMNA LAD previously mapped by us by chromatin immunoprecipitation (ChIP) sequencing (ChIP-seq) of LMNA in ASCs (Fig. 4 A; Rønningen et al., 2015). Interestingly, however, this inter-LAD region is punctually associated with LMNA (Fig. 4 A, top and magnified sections). To determine whether this LMNA association might play a regulatory role on *MIR335* gene activity, we first examined by ChIP-qPCR the binding of LMNA at four proximal sites >2 kb upstream of the *MIR335* transcription start site (TSS) within *MEST* introns 1 and 2 at four stages of adipogenic differentiation (Fig. 4 A). This region was chosen because binding of LMNA to promoters in ASCs has been shown to correlate with inactivity of their cognate genes (Lund et al., 2013). Consistent with ChIP-seq profiles, ChIP-qPCR showed low-level association of LMNA in the *MIR335* proximal promoter region in undifferentiated ASCs, yet this association was slightly above those detected at a control nonlamin-bound site (Lam−) and in IgG ChIPs (Fig. 4 B). Thus, although the *MEST/MIR335* locus was localized between two LMNA LADs, it appeared to punctually interact with low levels of LMNA in undifferentiated ASCs.

Adipogenic induction elicits a remodeling of the association of LMNA with the *MEST/MIR335* locus. Accordingly,
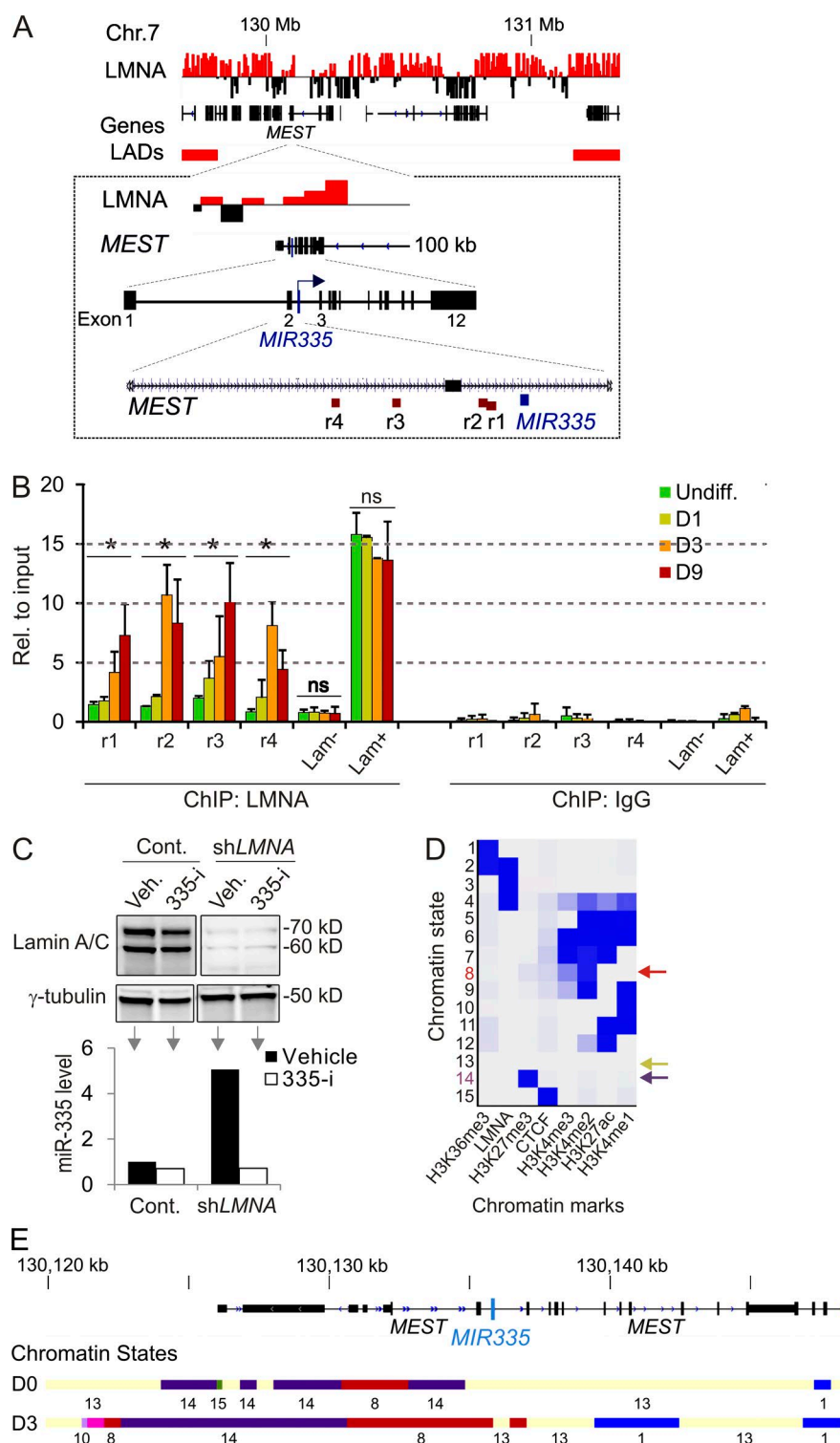
Figure 4. **Association of LMNA with the *MEST/ MIR335* locus contributes to miR-335 repression after adipogenic induction.** (A) Position of the *MEST/MIR335* locus between two LMNA LADs in ASCs: LMNA enrichment (ChIP/input ratios) and corresponding LADs (red bars) were identified by LMNA ChIP-seq in ASCs in a previous study (Rønningen et al., 2015). The magnified portion shows LMNA enrichment in 10-kb bins on the *MEST/MIR335* locus. The bottom panel shows the position of regions r1–r4 examined by ChIP in this study. (B) ChIP-qPCR analysis of LMNA on regions r1–r4 and control (Lam− and Lam+) sites in undifferentiated and differentiated (day 1–9) native ASCs; IgG control ChIPs are also shown (means ± SD of three biological replicates; ANOVA p-values: r1, *, $P = 0.007$; r2, *, $P = 0.002$; r3, *, $P = 0.018$; r4, *, $P = 0.010$). (C) Knockdown of LMNA up-regulates miR-335 in ASCs; top, Western blot of LMNA using anti-LMNA antibodies; bottom, miR-335 RT-qPCR in control and *LMNA* shRNA–treated cells exposed to a vehicle control or to 500 nM 335-i (mean of a duplicate analysis). (D) Chromatin state analysis of the *MEST/MIR335* locus in ASCs. Emission parameters for a 15-chromatin-state Hidden Markov model learned from combinations of indicated chromatin marks. Arrows point to chromatin states shown in the same color in panel E. (E) Genome browser view of chromatin states on the *MEST/MIR335* locus in ASCs before (day 0; D0) and after (day 3; D3) adipogenic induction. Numbers are color coded and correspond to chromatin state numbers in panel D.

we found a significant increase in LMNA association with the *MIR335* promoter region as a whole ($P < 0.001$; ANOVA; Fig. 4 B, r1–r4) and in each region examined individually ($P = 0.002–0.018$; ANOVA). This LMNA association anticorrelated with the down-regulation of miR-335 that followed adipogenic induction (see Fig. 2 C). In addition, knockdown of LMNA in ASCs led to miR-335 up-regulation (Fig. 4 C), suggesting a repressive role of LMNA on miR-335 expression. To examine this further, we used a machine learning approach to generate a Hidden Markov model of 15 chromatin states from recurrent combinations of seven chromatin marks previously mapped by ChIP-seq in ASCs and adipocytes (Fig. 4 D; Shah et al., 2014). These data show that the *MEST/MIR335* locus is predominantly marked by polycomb-mediated H3K27me3 (chromatin states 8 and 14; Fig. 4 E). After induction of differentiation, the locus retained its repressive state, in line with the further down-regulation of miR-335. Thus, LMNA binding to the *MEST/MIR335* locus in ASCs is linked to a repressive chromatin state at the locus.
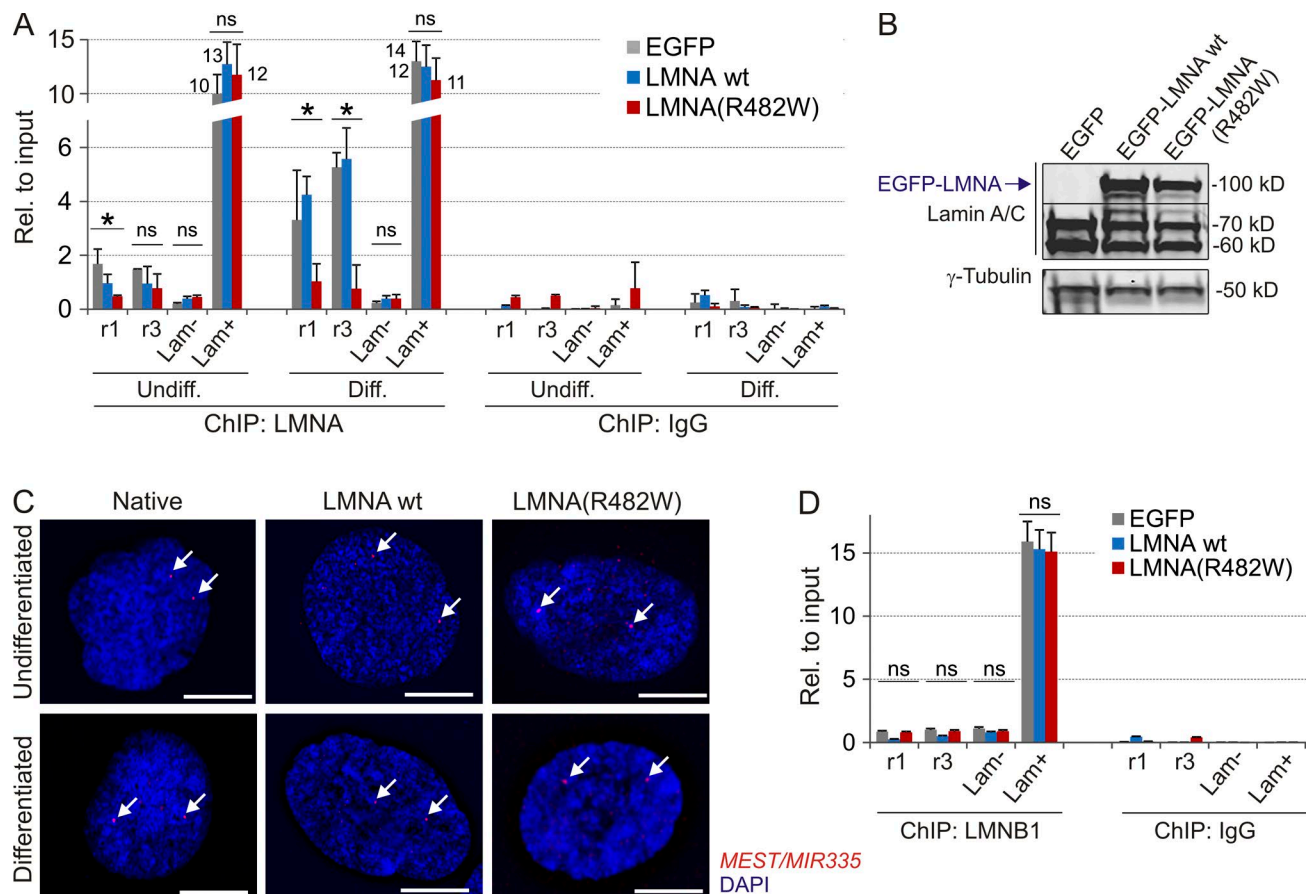
Figure 5. **WT LMNA and LMNA(R482W) differentially associate with the *MEST/MIR335* locus after adipogenic induction.** (A) ChIP-qPCR analysis of LMNA in undifferentiated and differentiated ASC^{EGFP}, ASC^{LMNAWT}, and ASC$^{LMNA(R482W)}$ (means ± SD of biological triplicates; ANOVA p-values: r1 Undiff., *, P = 0.026; r1 Diff., *, P = 0.003; r3 Diff., *, P = 0.001; ^{ns}P > 0.1). (B) Western blot assessment of expression of LMNA WT and R482W in ASCs. (C) FISH analysis of the *MEST/MIR335* locus (arrows) in native ASCs, ASC^{LMNAWT}, and ASC$^{LMNA(R482W)}$ before and after 3 d of adipogenic induction. DNA was stained with DAPI. Bars, 5 µm. (D) ChIP-qPCR analysis of LMNB1 in ASC^{EGFP}, ASC^{LMNAWT}, and ASC$^{LMNA(R482W)}$ (^{ns}ANOVA p-values ~1.000; means ± SD of triplicate ChIPs).

LMNA does not bind the MEST/MIR335 locus in ASCs expressing the FPLD2-causing LMNA(R482W) mutation

In light of these findings, we anticipated a differential LMNA association with the *MIR335* promoter in ASC$^{LMNA(R482W)}$, in which miR-335 is up-regulated. Indeed, we detected by ChIP no LMNA association with the promoter region (r1 and r3 sites) in undifferentiated ASC$^{LMNA(R482W)}$, whereas ASC^{LMNAWT} showed moderate binding (Fig. 5 A, Undiff.). These differences were not caused by variations in total cellular LMNA levels, which were similar between cell types (Fig. 5 B). After 3 d of adipogenic induction, however, LMNA became markedly enriched on the *MIR335* promoter in ASC^{LMNAWT}, whereas it remained near background in ASC$^{LMNA(R482W)}$ (P = 0.002–0.01; ANOVA; Fig. 5 A, Diff., and Fig. S2 C). Interestingly, in ASCs expressing the EDMD LMNA(R453W) mutation, LMNA binding to the *MIR335* promoter also increased during adipogenic induction to the same extent as with WT LMNA (Fig. S2 C). We conclude that the FPLD2 LMNA(R482W) mutation prevents association of LMNA with the *MIR335* locus upon adipogenic induction, whereas LMNA WT or R453W was not inhibitory. Given the correlation between LMNA binding to promoters and gene inactivity (Lund et al., 2013), these results are consistent with the high miR-335 levels in ASC$^{LMNA(R482W)}$ after induction

of differentiation and with the return of these levels to baseline in cells expressing LMNA WT or R453W.

Because LMNA binding to the *MIR335* locus is lower in ASC$^{LMNA(R482W)}$, we determined in a control experiment whether the R482W mutation would impair antibody binding, and thus pulldown efficiency, in ChIP assays. First, we found that LMNA similarly bound to a consensus LAD in both in undifferentiated and differentiated ASC^{EGFP}, ASC^{LMNAWT}, and ASC$^{LMNA(R482W)}$ (Fig. 5 A, Lam+) but not to a negative control site (Lam−). Next, we performed ChIP on LMNA from two normal and three LMNA p.R482W FPLD2 patient fibroblast cultures. These data revealed similar LMNA detection levels for a panel of genic and intergenic sites previously shown to be bound by LMNA in both cell types and differences at other sites predicted to show differential binding (Fig. S3 A; Paulsen et al., 2017). Thus, weaker LMNA detection on the *MIR335* locus in ASC$^{LMNA(R482W)}$ was not caused by lower antibody affinity for the mutant lamin in the ChIP assay. These data reinforce our conclusion that LMNA fails to associate with the *MIR335* locus in differentiated ASCs expressing the FPLD2 LMNA(R482W) mutation in contrast with those expressing WT LMNA or the EDMD LMNA(R453W) mutant.

We next examined whether association of LMNA with *MIR335* led to a repositioning of the locus in the nucleus with

respect to the nuclear periphery. FISH identified *MEST/MIR335* in the nuclear interior in native undifferentiated ASCs (Figs. 5 C and S4). Differentiation elicited a global shift of the locus away from the nucleus center ($P = 0.019$; Fisher's exact test), albeit with no repositioning at the nuclear periphery. Expression of LMNA WT also globally drew the locus away from the nucleus center compared with native ASCs ($P = 10^{-5}$), yet again without relocalizing the locus to the periphery; strikingly, this shift was not seen with LMNA(R482W) ($P = 0.360$; Fig. S4). These observations are consistent with the existence of an intranuclear pool of LMNA not localized at the nuclear envelope (Lund et al., 2013, 2015; Gesson et al., 2016). Moreover, differentiation tends to reposition the *MEST/MIR335* locus in native ASCs or ASC^{LMNAWT} but not in ASC$^{LMNA(R482W)}$; however, no differences in radial distributions were detectable between cell types (Figs. 5 C and S4). Corroborating the lack of association of *MEST/MIR335* with the nuclear periphery, we found by ChIP that lamin B1, which localizes at the nuclear envelope, did not interact with the *MIR335* promoter in cells expressing LMNA WT or R482W (Fig. 5 D).

Collectively, these findings suggest that expression of LMNA WT or R482W differentially reorganizes the genome. They suggest a dominant-negative effect of the R482W mutant on LMNA binding to the *MEST/MIR335* locus and thereby on transcriptional repression of the anti-adipogenic miR-335 after adipogenic induction.

LMNA(R482W) elicits H3K27 acetylation on predicted MIR335 enhancers after adipogenic induction

LMNA binding to promoters bears a repressive effect on gene expression (Lund et al., 2013). In addition, LMNA is required for proper compartmentalization of the Polycomb repressor complex PRC2 (Cesarini et al., 2015), which trimethylates H3K27. This raises the hypothesis that LMNA(R482W) may epigenetically modulate miR-335 expression. To test this, we assessed by ChIP H3K27me3 and H3K27ac enrichment upstream of *MIR335* in ASC^{LMNAWT} and ASC$^{LMNA(R482W)}$ before and after adipogenic induction. We examined the four proximal promoter sites upstream of the *MIR335* TSS (regions r1–r4; Table S1). We also searched for putative *MIR335* short- and long-range enhancers: to this end, we combined chromatin state modeling data from ENCODE ChIP-seq experiments showing enrichment in H3K4me1 and/or H3K27ac, histone modifications found on inactive and active enhancers, respectively (Fig. S5 A), with ENCODE genome-wide chromosome conformation capture of Hi-C data (Rao et al., 2014). The Hi-C data reveal multiple pairwise interactions of these predicted enhancers with the *MIR335* promoter (Fig. S5, B–D), providing six *MIR335*-predicted distal enhancer sites (regions r6–r11; Fig. S5 D).

In undifferentiated ASCs, H3K27me3 enrichment was similar across *MIR335* promoter sites as a whole (r1–r4; $P = 0.306$; ANOVA) and across enhancer sites as a whole (r6–r11; $P = 0.169$; ANOVA) regardless of expression of WT LMNA or LMNA(R482W) (Fig. 6 A). This suggests that differential *MIR335* expression in ASC$^{LMNA(R482W)}$ does not involve differential repression of *MIR335* by the PRC2 complex. H3K27ac patterns were also similar between ASC^{LMNAWT} and ASC$^{LMNA(R482W)}$ across promoter sites as a whole (r1–r4; $P = 0.200$; ANOVA; Fig. 6 B). However, we found an impact of LMNA(R482W) on H3K27ac on distal sites as a whole (r6–r11; $P = 0.001$; ANOVA; Fig. 6 B); this was caused by the H3K27-acetylated state at two enhancer

sites in particular, at −6.4 kb (r6) and −64.5 kb (r9) upstream of the *MIR335* TSS in ASC$^{LMNA(R482W)}$ compared with controls (Fig. 6 B; $P < 0.01$; post-ANOVA t tests). H3K27 acetylation of these enhancers suggests that they are active and was consistent with stronger miR-335 expression in these cells.

Adipogenic induction elicits cell type– and site–specific changes in H3K27 methylation and acetylation concordant with higher miR-335 levels in ASC$^{LMNA(R482W)}$. We found global H3K27 acetylation specifically in ASC$^{LMNA(R482W)}$ on promoter sites (r1–r4; $P = 0.002$; ANOVA) and enhancer sites (r6–r11; $P < 0.001$; ANOVA; Fig. 6 B). In particular, we identified in differentiated cells five distal sites (r6–r9 and r11) with increased H3K27ac specifically in ASC$^{LMNA(R482W)}$ ($P < 0.05$; post-ANOVA t tests; Fig. 6 B). Among these sites, three enhancers were acetylated after differentiation (r7, r8, and r11; §$P < 0.01$; Fisher's exact tests compared with the same sites in undifferentiated cells; Fig. 6 B). This de novo acetylation was accompanied by H3K27 demethylation at two sites in ASC$^{LMNA(R482W)}$ compared with undifferentiated cells (r8 and r11; §$P < 0.05$; Fisher's exact test; Fig. 6 A), resulting in an H3K27 unmethylated locus in LMNA$^{LMNA(R482W)}$ ($P < 0.05$; post-ANOVA t tests; Fig. 6 A). In contrast, a trend (albeit not statistically significant) toward increased H3K27me3 on *MIR335* proximal and distal regions in ASC^{LMNAWT} after differentiation exacerbated cell type differences in H3K27me3, with specific enhancers being H3K27 trimethylated in ASC^{LMNAWT} and ASC controls compared with LMNA$^{LMNA(R482W)}$ (r6–r11; $P < 0.01$; post-ANOVA t tests; Fig. 6 A). Changes in H3K27me3 and H3K27ac between cell types were validated by their expected enrichment on a housekeeping gene (*GAPDH*) and on a non-expressed myogenic gene (*MYOG*; Fig. S3 B).

Additionally, testing the specificity of H3K27 acetylation events for the R482W mutation, we also examined ASC$^{LMNA(R453W)}$. We found overall no significant differences in H3K27ac on *MIR335* promoter and enhancer sites between ASC$^{LMNA(R453W)}$ and native ASCs regardless of differentiation status (Fig. S2 D). One noticeable difference, however, was that hyperacetylation of one enhancer (r6) in undifferentiated ASC$^{LMNA(R453W)}$ (Fig. S2 D), which was consistent with the overexpressed state of miR-335 in these cells (Fig. S2 A), was similar to ASC$^{LMNA(R482W)}$. We also observed lower H3K27ac on enhancers in differentiated ASC$^{LMNA(R453W)}$ compared with ASC$^{LMNA(R482W)}$ ($P < 0.05$; Fisher's exact tests; Fig. S2 E, sites r6, r9, and r10), in line with normalized expression of miR-335 in differentiated LMNA(R453W) mutants (Fig. S2 A).

We conclude that although *MIR335* promoter and enhancer elements are similarly H3K27 methylated globally in undifferentiated ASCs expressing WT LMNA or LMNA(R482W), two enhancers were already acetylated in the mutants. Differentiation elicited H3K27 methylation of proximal and distal regulatory elements in cells expressing WT LMNA and in contrast, H3K27 acetylation in cells expressing the R482W mutation. Acetylation of one enhancer in particular (r6, ~6.5 kb upstream of the *MIR335* gene) specific to undifferentiated cells expressing R482W or R453W correlated with the overexpressed state of miR-335 in these cells; this suggests an important role of this enhancer element in the activity of the *MIR335* gene.

LMNA(R482W) elicits a remodeling of MIR335 promoter–enhancer conformation

Acetylation of H3K27 on *MIR335* enhancers detected in ASC$^{LMNA(R482W)}$ after adipogenic induction suggests interac-
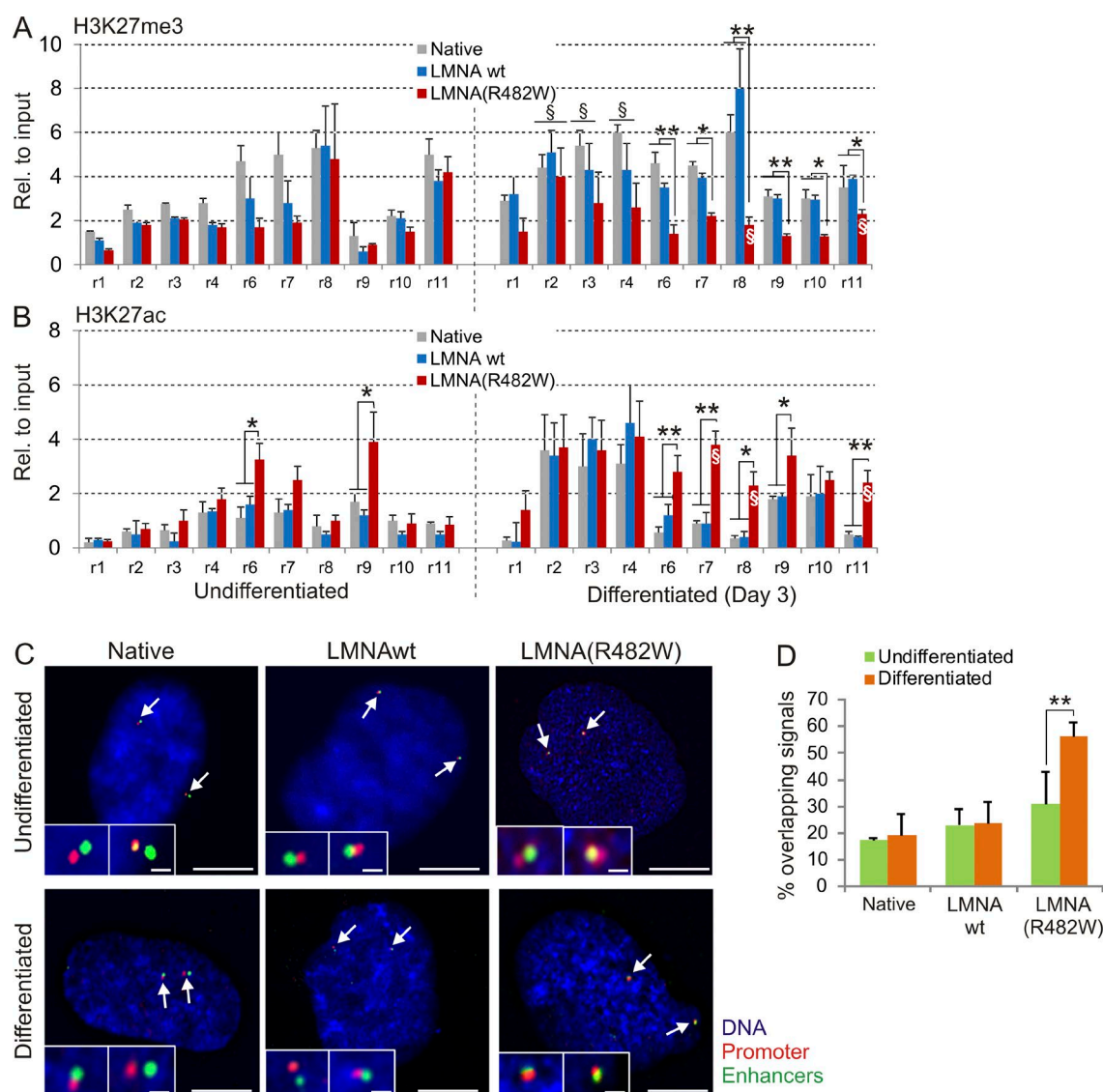
Figure 6. **LMNA(R482W) elicits H3K27 acetylation of predicted *MIR335* enhancers after induction of differentiation.** (A and B) H3K27me3 (A) and H3K27ac (B) enrichment determined by ChIP-qPCR upstream of *MIR335* in undifferentiated and differentiated (day 3) ASCs, ASC^LMNAWT, and ASC^LMNA(R482W) (means ± SD of duplicate transductions and differentiations, each analyzed by duplicate ChIP). Values for IgG ChIPs for all regions and cell types ranged from 0.02 to 0.24 and are not depicted. Statistics for A: one-way ANOVA on r1–r4 Undiff., P = 0.306; r6–r11 Undiff., P = 0.169; r1–r4 Diff., P = 0.200; and r6–r11 Diff., P = 0.001. §P < 0.01, Fisher's exact tests relative to the same undifferentiated cell type: *, P < 0.05; **, P < 0.01; post-ANOVA *t* tests. (B) One-way ANOVA on r1–r4 Undiff., P = 0.300; r6–r11 Undiff., P = 0.001; r1–r4 Diff., P = 0.002; and r6–r11 Diff., P < 0.001; §P < 0.01, Fisher's exact tests relative to the same differentiated cell type; *, P < 0.05; **, P < 0.01; post-ANOVA *t* tests. (C) Dual-color FISH analysis of the *MIR335* gene (red signals) and *MIR335* enhancer regions r10 and r11 (green signals) in native ASCs, ASC^LMNAWT, and ASC^LMNA(R482W) before and after a 3-d adipogenic induction. Representative views are shown. Bars: (main images) 5 µm; (insets) 0.5 µm. (D) Quantification of FISH observations (*n* = 44–64 alleles analyzed in two independent FISH analyses; means ± SD; **, P = 0.0082; Fisher's exact test).

tions with the *MIR335* promoter by chromatin looping (Zhang et al., 2013). We tested this hypothesis by two-color FISH using distinctly labeled promoter and enhancer probes. Probes were generated to cover the *MIR335* gene and promoter as well as the distal enhancer element r11 located ∼200 kb upstream of *MIR335*. In both undifferentiated and differentiated ASCs that were either native or expressing WT LMNA, these promoter and enhancer elements displayed a relatively low incidence of colocalization on the majority of alleles (∼80%; Fig. 6, C and D). This was also seen in undifferentiated ASC^LMNA(R482W), where we detected 30% probe overlap (Fig. 6, C). After induction of differentiation, however, this proportion markedly increased to 56% of alleles in the LMNA(R482W) mutants, reflecting interaction of a high proportion of *MIR335* promoter

and enhancer sites (Fig. 6, C and D). Importantly, these results support implications from the increase in H3K27 acetylation detected on *MIR335* enhancers after adipogenic induction of ASCs expressing the lipodystrophic R482W mutation. They also strongly suggest a conformational change of the *MEST/ MIR335* locus, which does not take place to the same extent in cells expressing WT LMNA.

Discussion

A pending question in our understanding of laminopathies is how phenotypes emerge in specific tissues of predominantly mesenchymal origin. Cellular defects contributing to the
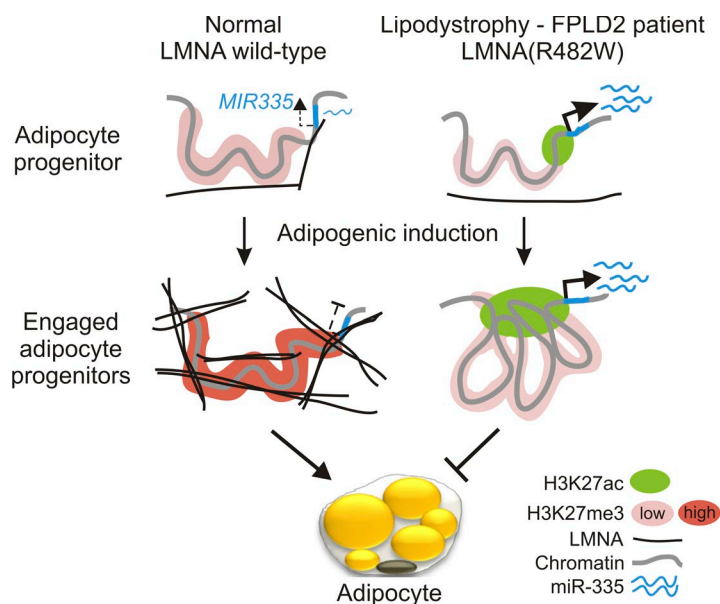
Normal
LMNA wild-type

Lipodystrophy - FPLD2 patient
LMNA(R482W)

Adipocyte progenitor

MIR335

Adipogenic induction

Engaged adipocyte progenitors

Adipocyte

H3K27ac
H3K27me3 low | high
LMNA
Chromatin
miR-335

Figure 7. **Model of differential LMNA association and epigenetic regulation of miR-335 in ASCs expressing WT LMNA or the lipo-dystrophic LMNA(R482W) mutation.** In WT ASCs, LMNA binding to the MIR335 locus after induction of adipogenic differentiation coincides with enhanced H3K27 trimethylation and transcriptional repression of MIR335. In cells expressing the lipodystrophy-causing LMNA(R482W) hot-spot mutation, MIR335 is overexpressed, in line with H3K27 acetylation of promoter and enhancer sites. Lack of LMNA binding after induction of differentiation of the mutant ASCs enables H3K27 acetylation on several enhancer sites. This favors a looping of these enhancers onto the MIR335 promoter, as shown in this study by FISH, enabling a persistence of MIR335 transcription. Overexpression of miR-335 prevents differentiation of adipocyte progenitors into adipocytes, which is consistent with the lipoatrophy phenotype of FPLD2 patients (bottom; lipid droplets and the nucleus are represented by yellow and brown spheroids in the adipocyte, respectively).

FPLD2 phenotype (Oldenburg et al., 2014; Osmanagic-Myers et al., 2015; Vadrot et al., 2015; Le Dour et al., 2017) are underlined by a disorganization of the nuclear lamina (Vigouroux et al., 2001; Caron et al., 2007), which impacts spatial genome conformation through altered LMNA–chromatin interactions (Perovanovic et al., 2016; Paulsen et al., 2017). We now show a dominant-negative effect of the FPLD2-causing LMNA p.R482W mutation on chromatin organization and epigenetic states regulating expression of the anti-adipogenic microRNA miR-335 in human adipocyte progenitors.

Our findings have implications in the etiology of lipodystrophic laminopathies. Although our experimental model lacks the context of the whole organism and of the depot-specific phenotype, ASCs used in this study are relevant for investigations of molecular mechanisms of FPLD2 because they originate from gluteofemoral fat depots, which are lipoatrophic in patients. ASCs expressing LMNA(R482W) show adipogenesis impairment, myogenic gene induction (Oldenburg et al., 2014), and alterations in lamin–chromatin interactions consistent with predictions from 3D genome structures modeled from FPLD2 patient cells (Paulsen et al., 2017). In addition, ASC[LMNA(R482W)] overexpresses miR-335, which is not only anti-adipogenic (Tomé et al., 2011) but is also implicated in metabolic disorders (Fernández-Hernando et al., 2011) and in skeletal muscle development (Meyer et al., 2015). Moreover, we show that miR-335 positively regulates translation of the promyogenic factor FXR1P in these cells and in FPLD2 patient fibroblasts. These observations raise the hypothesis that miR-335 overexpression may contribute to the lipoatrophic and myogenic phenotype of FPLD2 patients and implicate miR-335 in the pathophysiology of the disease.

We propose a model of how A-type lamins may modulate adipogenic differentiation via a regulation of epigenetic states and chromatin conformation at the *MIR335* locus in adipocyte progenitors (Fig. 7). In undifferentiated cells, punctual WT LMNA binding to the locus coincides with basal *MIR335* gene expression. The FPLD2-causing LMNA(R482W) mutation, however, prevents LMNA binding to *MIR335*, and acetylation of two enhancer elements prompts *MIR335* overexpression (Fig. 7). Interestingly, *MIR335* enhancer acetylation (but on one

site only) also occurs with the EDMD-causing LMNA(R453W) mutation and coincides with overexpressed miR-335. This suggests that in undifferentiated ASCs, the acetylation state of a minimal set of *MIR335* enhancers, rather than minimal LMNA association by itself, is important to regulate *MIR335* expression. Moreover, high miR-335 levels in undifferentiated ASCs do not per se compromise the efficiency of adipogenic induction. Rather, the dynamics of the epigenome and local chromatin rearrangement at the *MIR335* locus are essential for *MIR335* inactivation, keeping miR-335 levels low, and are critical for differentiation.

Indeed, after adipogenic induction, a network of LMNA forms around the locus in WT cells, where it presumably stabilizes the PRC2 complex recruited to methylate H3K27. Transcriptional inhibition of *MIR335* keeps miR-335 levels low, enabling adipogenesis (Fig. 7). The LMNA(R453W) mutation does not impair LMNA association with *MIR335*, favoring *MIR335* repression and adipogenic differentiation. In sharp contrast, in the presence of the lipodystrophic R482W mutation, LMNA is unable to tether *MIR335*, impairing PRC2 engagement and H3K27 methylation at the locus (Fig. 7). Instead, H3K27 acetylation detected across the *MIR335* promoter and on multiple enhancers may be facilitated by the absence of LMNA, possibly by displacement of histone deacetylases reported to be enriched in the vicinity of LMNA (Demmerle et al., 2012). H3K27 hyperacetylation on multiple regulatory elements predicts promoter–enhancer interactions through the formation of chromatin loops as suggested by our FISH data. This conformation change is consistent with the overexpressed state miR-335 in LMNA(R482W) mutant ASCs and with subsequent inhibition of adipogenic differentiation (Fig. 7). The absence of an LMNA network tethering the *MIR335* locus may facilitate these promoter–enhancer interactions because of increased chromatin mobility in a less constrained environment (Bronshtein et al., 2015).

This local effect on chromatin conformation is likely part of a large-scale reorganization of the lamina–chromatin interaction network as we have modeled from 3D genome structures in FPLD2 patient cells (Paulsen et al., 2017). This may entail weaker interactions of the mutated R482W residue on the surface

of the immunoglobulin fold of LMNA, with DNA and nucleosomes, as shown in vitro (Stierlé et al., 2003; Duband-Goulet et al., 2011). Alternatively, accumulation of immature pre-LMNA at the nuclear envelope reported in adipose tissue of FPLD2 patients (Caron et al., 2007) may sequester of a pool of intranuclear LMNA away from genes it would otherwise associate with and regulate (Naetar et al., 2008; Naetar and Foisner, 2009; Lund et al., 2013; Rønningen et al., 2015; Gesson et al., 2016).

Our findings raise the issue of how broad the implications of disrupting the LMNA network on Polycomb-mediated gene repression might be. A-type lamins constrain chromatin (Bronshtein et al., 2015) and are essential for proper PRC2 targeting (Cesarini et al., 2015), and thus deregulation of H3K27 methylation or acetylation may widely impact enhancer–promoter interactions. Deregulation of PRC2 targeting may also directly alter adipogenic gene expression. Adipogenesis is impaired by Wnt signaling (Rosen and MacDougald, 2006), which is under transcriptional control of PRC2 repressing a subset of *Wnt* genes in the mouse (Wang et al., 2010; Hemming et al., 2014; Yi et al., 2016). Defective Polycomb-mediated repression of *WNT* genes in gluteofemoral adipocyte progenitors with the LMNA p.R482W mutation may hamper differentiation in the context of lipodystrophic laminopathies.

Alterations in spatial chromatin organization as an important disease-causing factor are becoming increasingly evident. Physical disruption of topologically associated domains, the building blocks of chromatin (Gibcus and Dekker, 2013), by point mutations, chromosomal deletions, or inversions has been causatively linked to developmental disorders (Lupiáñez et al., 2016). Together with the role of A-type lamins in constraining chromatin and in regulating local and large-scale genome conformation, our findings provide evidence for perturbations in 3D genome organization as a significant causing factor of tissue type–specific disorders that characterize laminopathies.

Materials and methods

Cells, transfections, and reagents

Skin fibroblasts were purchased from Lonza (CTL 1; CC-2512) or were from a healthy donor (CTL 2) and FPLD2 patients with the LMNA p.R482W mutation (Decaudain et al., 2007). All fibroblasts were cultured in DMEM/F12 containing 10% fetal calf serum and were used at passages 4–7 (Oldenburg et al., 2014). FPLD2 patient fibroblasts were provided by C. Vigouroux (Hôpital Saint Antoine, Paris, France) and studies were approved by the Institutional Review Board of Hôpital Saint Antoine.

ASCs previously isolated from gluteofemoral fat obtained by liposuction (approval by the Regional Committee for Research Ethics for Southern Norway; Boquest et al., 2005) were cultured under proliferative conditions in DMEM/F12 (17.5 mM glucose) with 10% fetal calf serum, 10 ng/ml epidermal growth factor, and 20 ng/ml basic fibroblast growth factor. Upon confluence and after growth factor removal for 48 h, cells were differentiated into adipocytes with a cocktail of 0.5 µM 1-methyl-3 isobutyl xanthine, 1 µM dexamethasone, 10 µg/ml insulin, and 200 µM indomethacin for the indicated time periods up to 9 d. ASCs were transduced using lentiviruses to express EGFP, EGFP-LMNA WT, or EGFP-LMNA(R482W) as described previously (Oldenburg et al., 2014). In brief, ASCs were transduced and cultured with 1.5 mg/ml puromycin for 8 d to select expressing cells and maintained in culture with 0.1 mg/ml puromycin. EGFP-LMNA (WT or mutant) expression was induced with 1 mg/ml doxycycline.

DT40 Dicer Eta 8–25 060414 cells were a gift from T. Fukagawa (National Institute of Genetics, Mishima, Japan). Transfections of 335-i (500 nM) or 335-m (500 nM) were done by nucleofection (Lonza) using H_2O as vehicle. The MG132 proteasome inhibitor was purchased from VWR.

RT-PCR

Total mRNA was isolated using an RNeasy kit (QIAGEN), and 1 µg RNA was used for cDNA synthesis (Bio-Rad Laboratories). RT-qPCR was done using IQ SYBR green (Bio-Rad Laboratories) and *GAPDH* as reference gene. PCR conditions were 95°C for 3 min and 40 cycles of 95°C for 30 s, 60°C for 30 s, and 72°C for 30 s (Oldenburg et al., 2014). miRNAs were isolated using the mirVANA miRNA isolation kit (Invitrogen), and miR-335 was quantified by TaqMan assays using the U6 RNA as reference. RT-PCR primers are listed in Table S2.

Immunoblotting

Proteins were resolved by 10% SDS-PAGE, transferred onto Immobilon-FL membranes (EMD Millipore), and blocked with Odyssey blocking buffer (LI-COR Biosciences). Immunoblotting was done using antibodies to LMNA (mouse; sc-7292; LI-COR Biosciences), EGFP (mouse; clones 7.1 and 13.1; Roche), FXR1P (goat; sc-10554; Santa Cruz Biotechnology, Inc.), P53 (mouse; sc-126; Santa Cruz Biotechnology, Inc.), DICER (rabbit; sc-30226; Santa Cruz Biotechnology, Inc.), and γ-tubulin (mouse; T5326; Sigma-Aldrich). Densitometry analysis was done using ImageJ (v.1.48; National Institutes of Health).

In-cell Western blotting

ASCs were cultured to confluence in 24-well plates and induced to differentiate into adipocytes as described in the Cells, transfections, and reagents section. Cells were fixed in 3.7% formaldehyde in PBS for 20 min at room temperature and washed 5× in 0.1% Triton X-100/PBS. Cells were blocked with Odyssey blocking buffer for 1 h, incubated overnight with antiperilipin antibody (rabbit; 2 µg/ml diluted in Odyssey blocking buffer; D418; Cell Signaling Technology) at 4°C, washed 5× with 0.1% Tween-20/PBS, and incubated for 1 h at room temperature with secondary antibody (IRDye800-conjugated donkey anti–rabbit; 1:800) and 5 µM DRAQ5 as DNA stain, in Odyssey blocking buffer/0.2% Tween-20. Cells were washed 5× in 0.1% Tween-20/PBS, and the plate was imaged on the Odyssey scanner. Efficiency of adipogenic induction was determined by the ratio of perilipin/Draq5 signal in duplicate experiments.

ChIP

ChIP of LMNA (antibody to LMNA; 10 µg; mouse; sc-7292; Santa Cruz Biotechnology, Inc.), LMNB1 (10 µg; rabbit; ab16048; Abcam), H3K27me3 (2.5 µg; rabbit; C15410069; Diagenode), H3K27ac (2.5 µg; rabbit; C15410174; Diagenode), and relevant control ChIPs (mouse or rabbit IgG; 2.5 µg) were done in two to five replicates from 2×10^6 cells per ChIP (Rønningen et al., 2015). Cells were cross-linked with 1% formaldehyde for 10 min, lysed for 10 min in ChIP lysis buffer (1% SDS, 10 mM EDTA, 50 mM Tris-HCl, pH 7.5, proteinase inhibitors, and 1 mM PMSF) and sonicated 4× for 10 min in a Bioruptor (Diagenode) to generate 200–500-bp DNA fragments. After sedimentation at 10,000 *g* for 10 min, the supernatant was collected and diluted 10× in RIPA buffer (140 mM NaCl, 10 mM Tris-HCl, pH 8.0, 1 mM EDTA, 0.5 mM EGTA, 1% triton X-100, 0.1% SDS, 0.1% sodium deoxycholate, 1 mM PMSF, and protease inhibitors); this constituted the input chromatin fraction. Chromatin was incubated overnight at 4°C with a relevant primary antibody coupled to magnetic DynaBeads Protein A/G (Invitrogen). After magnetic isolation, ChIP samples were washed 4× in ice-cold RIPA buffer. Cross-links were reversed, and DNA was eluted for 6 h at 68°C in

50 mM NaCl, 20 mM Tris-HCl, pH 7.5, 5 mM EDTA, 1% SDS, and 50 ng/µl proteinase K. DNA was purified and dissolved in H_2O. ChIP DNA was used as template for qPCR. PCR was done using SYBR green (Bio-Rad Laboratories) with 95°C for 3 min and 40 cycles of 95°C for 30 s, 60°C for 30 s, and 72°C for 30 s, using ChIP primers listed in Table S1.

Luciferase assay

The LightSwitch *FXR1* 3′ UTR luciferase reporter was from Switch-Gear Genomics. The *FXR1* 3′ UTR was deleted of the miR-335 target sequence at position −322 by site-directed mutagenesis using primers 5′-TGGGTGGGGTGGGATCCCTAATTAGCTGCTTTTGTTACAT-3′ and 5′-ATGTAACAAAAGCAGCTAATTAGGGATCCCACCCCACCCA-3′. DT40 cells knocked down of DICER for 96 h (Fukagawa et al., 2004) were cotransfected by nucleofection using 20 µg luciferase reporter and 5 µM hsa–335-m. After 24 h, luciferin was added, and luminescence was measured using an IVIS Spectrum µCT camera and the LivingImage v.431 software (PerkinElmer). Luminescence from transfected fibroblasts was assayed with the LightSwitch Luciferase Assay kit (Active Motif) and measured by Fluostar optima (BMG LABTECH).

Bisulfite sequencing

Genomic DNA was purified and bisulfite treated using MethylEasy (Human Genetic Signatures). Converted DNA was amplified by PCR using primers designed with MethPrimer (Li and Dahiya, 2002) to include 6 CpGs in the *MIR335* promoter (forward, 5′-TTTTTGTTTTTTTTATAGGATGAGG-3′, and reverse, 5′-ACAAATTAAAATCTCAATCCCTACC-3′; position of amplicon relative to *MIR335* TSS: nucleotides −761 to −389 [nucleotides 130, 135, 191–130, 135, and 564 on chromosome 7; hg19]). PCR conditions were 95°C for 10 min and 35 cycles of 95°C for 1 min, 58°C for 2 min, and 72°C for 2 min followed by 10 min at 72°C. PCR products were cloned into *Escherichia coli*, and 10 clones were sequenced. The percentage of each methylated CpG across all sequenced clones was compared between donors using Fisher's exact tests and two-tailed p-values; no significant difference was found between cell types.

FISH

Cells were incubated in hypotonic buffer (0.25% KCl and 0.5% trisodium citrate) for 10 min, fixed in ice-cold methanol/acetic acid (3:1), and dropped on slides. A fosmid probe covering the *MIR335/MEST* gene (reference WI2-3174J24; BacPac Resource Center) was labeled with digoxigenin-11-dUTP (Roche), and a fosmid probe covering the *MIR335* enhancer region r11 (Chromosome 7, position 129,854,050–129,895,632; reference WI2-2199E12; BacPac Resource Center) was labeled with Biotin-16-dUTP (Roche). Per slide, 80 ng of each probe was mixed with 8 µg human Cot-1 DNA and 10 µg salmon sperm DNA and precipitated. The DNA pellet was dissolved in 16 µl hybridization mix (50% deionized formamide, 2× SSC, 1% Tween-20, and 10% dextran sulfate) at room temperature for 1 h. Slides were RNase treated and washed twice in 2× SSC, dehydrated in 70%, 90%, and 100% ethanol, and air dried. Slides were denatured for 1 min and 20 s in 70°C 70% deionized formamide/2× SSC, pH 7.5, dehydrated in ice-cold 70%, 90%, and 100% ethanol, and air dried. Probes were denatured for 5 min at 70°C and preannealed for 15 min at 37°C. 15 µl of probe was applied onto coverslips (22 × 22 mm), which were then mounted on a slide. Slides were hybridized overnight at 37°C and washed in 2× SSC (45°C for 4 × 3 min) and in 0.1× SSC (60°C for 4 × 3 min). Slides were blocked in 5% skim milk in 4× SSC for 5 min at 37°C and incubated at 37°C for 30–60 min with anti-digoxigenin (mouse; 0.4 µg/ml in blocking buffer; Roche). Slides were washed in 4× SSC/0.1% Tween-20 for 3 × 2 min and incubated with anti–mouse Alexa Fluor 594 (rabbit;

2.5 µg/ml in blocking buffer; Jackson ImmunoResearch Laboratories, Inc.) and Avidin Alexa Fluor 488 (1.7 µg/ml in blocking buffer; Invitrogen). Slides were washed and further incubated with anti–rabbit Alexa Fluor 594 (donkey; 2.5 µg/ml in blocking buffer; Jackson ImmunoResearch Laboratories, Inc.) and biotinylated anti–avidin D conjugate (goat; 1.0 µg/ml in blocking buffer; Vector Laboratories). Slides were washed, incubated with Avidin Alexa Fluor 488 (1.7 µg/ml; Invitrogen), washed, and mounted with 0.2 µg/ml DAPI in fluorescent mounting medium (Dako).

FISH images were acquired on an IX81 microscope (Olympus) fitted with epifluorescence, a 100× 1.4 NA objective mounted on a piezo drive, and a DeltaVision personalDV (Applied Precision, Ltd.) imaging station. Quantification of FISH probe distance to the nuclear periphery was done using ImageJ and with DAPI staining as a marker to the nucleus edge.

Chromatin states and identification of putative MIR335 enhancers

ChIP-seq data for H3K4me1, H3K4me2, H3K4me3, H3K27ac, H3K27me3, H3K36me3, CCCTC-binding factor, and LMNA in undifferentiated and differentiated ASCs were from previous studies (Mikkelsen et al., 2010; Rønningen et al., 2015). Peak calls and the machine learning algorithm ChromHMM (Ernst and Kellis, 2012) were used to identify chromatin states from the called peaks (Shah et al., 2014). Options were selected to learn a 15-state model using the Baum–Welch training algorithm (Miklós and Meyer, 2005).

To identify *MIR335* enhancers, H3K4me1/2/3, H3K27ac, H3K27me3, and H3K36me3 enrichment profiles in ASCs (Mikkelsen et al., 2010) as well as GM12878, HMEC, HUVEC, IMR90, K562, and NHEK (ENCODE Project Consortium, 2012) were modeled using ChromHMM to generate a four-chromatin-state model binned at 1 kb resolution. Chromatin state 1 was selected as an enhancer state, and enhancer states <1 kb apart were merged (Shah et al., 2014). The resulting predicted enhancer sites were used as potential sites of interaction with the *MIR335* promoter (defined as −4 to +1 kb around the *MIR335* TSS) with an arbitrary maximum distance of ±2 megabases (to avoid long-distance interactions) and a minimum distance of 8 kb from the *MIR335* promoter (to avoid counting self-ligating mate pairs). We then used genome-wide chromosome conformation to capture Hi-C data for GM12878, HMEC, HUVEC, IMR90, K562, and NHEK cells mapped at 1 kb resolution (Rao et al., 2014) to identify promoter–enhancer interactions. Using the *MIR335* promoter and putative enhancers as anchors for each promoter–enhancer pair, numbers of Hi-C interactions were counted, and the top six pairs with the highest numbers of counts were used to define the amplicons (r6–r11) analyzed by ChIP-qPCR in this study.

Data viewing

Browser views of gene tracks, ChIP-seq data, and chromatin states shown in Figs. 4 (A and D) and S5 (B–D) were prepared using the Integrated Genomics Viewer (Robinson et al., 2011). Genes were from Illumina iGenomes gene annotation with the UCSC genome browser for hg19.

Statistical analysis

For all experiments, numbers of replicates are indicated. Comparisons of miR-335 or mRNA levels or ChIP enrichment values between multiple samples were done using one-way ANOVA, and p-values are reported. Pairwise comparisons of samples after ANOVA were done using post-ANOVA *t* tests. Other pairwise comparisons were done using Fisher's exact tests, and p-values are reported. Units of values reported, numbers of replicates and statistical tests, and p-values are indicated in figure legends.

Online supplemental material

Fig. S1 shows FXR1P levels in FPLD2 patient cells and ASCs under different conditions as well as *MEST* mRNA levels and DNA methylation patterns. Fig. S2 shows data pertaining to ASCs expressing the EDMD LMNA(R453W) mutation. Fig. S3 shows control ChIP-qPCRs of LMNA in control and FPLD2 fibroblasts as well as ChIP-qPCRs of H3K27me3 and H3K27ac in ASCs. Fig. S4 shows distances of FISH probes to the nuclear periphery. Fig. S5 shows the approach used to identify *MIR335* enhancers putatively interacting with the *MIR335* promoter. Tables S1 and S2 list ChIP-qPCR and RT-qPCR primers, respectively.

References

Boguslavsky, R.L., C.L. Stewart, and H.J. Worman. 2006. Nuclear lamin A inhibits adipocyte differentiation: implications for Dunnigan-type familial partial lipodystrophy. *Hum. Mol. Genet.* 15:653–663. http://dx.doi.org/10.1093/hmg/ddi480

Boquest, A.C., A. Shahdadfar, K. Frønsdal, O. Sigurjonsson, S.H. Tunheim, P. Collas, and J.E. Brinchmann. 2005. Isolation and transcription profiling of purified uncultured human stromal stem cells: Alteration of gene expression after in vitro cell culture. *Mol. Biol. Cell.* 16:1131–1141. http://dx.doi.org/10.1091/mbc.E04-10-0949

Bronshtein, I., E. Kepten, I. Kanter, S. Berezin, M. Lindner, A.B. Redwood, S. Mai, S. Gonzalo, R. Foisner, Y. Shav-Tal, and Y. Garini. 2015. Loss of lamin A function increases chromatin dynamics in the nuclear interior. *Nat. Commun.* 6:8044. http://dx.doi.org/10.1038/ncomms9044

Calimlioglu, B., K. Karagoz, T. Sevimoglu, E. Kilic, E. Gov, and K.Y. Arga. 2015. Tissue-specific molecular biomarker signatures of type 2 diabetes: An integrative analysis of transcriptomics and protein–rotein interaction data. *OMICS.* 19:563–573. http://dx.doi.org/10.1089/omi.2015.0088

Caron, M., M. Auclair, B. Donadille, V. Béréziat, B. Guerci, M. Laville, H. Narbonne, C. Bodemer, O. Lascols, J. Capeau, and C. Vigouroux. 2007. Human lipodystrophies linked to mutations in A-type lamins and to HIV protease inhibitor therapy are both associated with prelamin A accumulation, oxidative stress and premature cellular senescence. *Cell Death Differ.* 14:1759–1767. http://dx.doi.org/10.1038/sj.cdd.4402197

Cesarini, E., C. Mozzetta, F. Marullo, F. Gregoretti, A. Gargiulo, M. Columbaro, A. Cortesi, L. Antonelli, S. Di Pelino, S. Squarzoni, et al. 2015. Lamin A/C sustains PcG protein architecture, maintaining transcriptional repression at target genes. *J. Cell Biol.* 211:533–551. http://dx.doi.org/10.1083/jcb.201504035

Cheever, A., and S. Ceman. 2009. Translation regulation of mRNAs by the fragile X family of proteins through the microRNA pathway. *RNA Biol.* 6:175–178. http://dx.doi.org/10.4161/rna.6.2.8196

Cheever, A., E. Blackwell, and S. Ceman. 2010. Fragile X protein family member FXR1P is regulated by microRNAs. *RNA.* 16:1530–1539. http://dx.doi.org/10.1261/rna.2022210

Davidovic, L., N. Durand, O. Khalfallah, R. Tabet, P. Barbry, B. Mari, S. Sacconi, H. Moine, and B. Bardoni. 2013. A novel role for the RNA-binding protein FXR1P in myoblasts cell-cycle progression by modulating *p21/Cdkn1a/Cip1/Waf1* mRNA stability. *PLoS Genet.* 9:e1003367. http://dx.doi.org/10.1371/journal.pgen.1003367

Decaudain, A., M.C. Vantyghem, B. Guerci, A.C. Hécart, M. Auclair, Y. Reznik, H. Narbonne, P.H. Ducluzeau, B. Donadille, C. Lebbé, et al. 2007. New metabolic phenotypes in laminopathies: LMNA mutations in patients with severe metabolic syndrome. *J. Clin. Endocrinol. Metab.* 92:4835–4844. http://dx.doi.org/10.1210/jc.2007-0654

Demmerle, J., A.J. Koch, and J.M. Holaska. 2012. The nuclear envelope protein emerin binds directly to histone deacetylase 3 (HDAC3) and activates HDAC3 activity. *J. Biol. Chem.* 287:22080–22088. http://dx.doi.org/10.1074/jbc.M111.325308

Duband-Goulet, I., S. Woerner, S. Gasparini, W. Attanda, E. Kondé, C. Tellier-Lebègue, C.T. Craescu, A. Gombault, P. Roussel, N. Vadrot, et al. 2011. Subcellular localization of SREBP1 depends on its interaction with the C-terminal region of wild-type and disease related A-type lamins. *Exp. Cell Res.* 317:2800–2813. http://dx.doi.org/10.1016/j.yexcr.2011.09.012

ENCODE Project Consortium. 2012. An integrated encyclopedia of DNA elements in the human genome. *Nature.* 489:57–74. http://dx.doi.org/10.1038/nature11247

Ernst, J., and M. Kellis. 2012. ChromHMM: automating chromatin-state discovery and characterization. *Nat. Methods.* 9:215–216. http://dx.doi.org/10.1038/nmeth.1906

Favreau, C., D. Higuet, J.C. Courvalin, and B. Buendia. 2004. Expression of a mutant lamin A that causes Emery-Dreifuss muscular dystrophy inhibits in vitro differentiation of C2C12 myoblasts. *Mol. Cell. Biol.* 24:1481–1492. http://dx.doi.org/10.1128/MCB.24.4.1481-1492.2004

Fernández-Hernando, C., Y. Suárez, K.J. Rayner, and K.J. Moore. 2011. MicroRNAs in lipid metabolism. *Curr. Opin. Lipidol.* 22:86–92. http://dx.doi.org/10.1097/MOL.0b013e3283428d9d

Fukagawa, T., M. Nogami, M. Yoshikawa, M. Ikeno, T. Okazaki, Y. Takami, T. Nakayama, and M. Oshimura. 2004. Dicer is essential for formation of the heterochromatin structure in vertebrate cells. *Nat. Cell Biol.* 6:784–791. http://dx.doi.org/10.1038/ncb1155

Gesson, K., P. Rescheneder, M.P. Skoruppa, A. von Haeseler, T. Dechat, and R. Foisner. 2016. A-type lamins bind both hetero- and euchromatin, the latter being regulated by lamina-associated polypeptide 2 alpha. *Genome Res.* 26:462–473. http://dx.doi.org/10.1101/gr.196220.115

Gibcus, J.H., and J. Dekker. 2013. The hierarchy of the 3D genome. *Mol. Cell.* 49:773–782. http://dx.doi.org/10.1016/j.molcel.2013.02.011

Hemming, S., D. Cakouros, S. Isenmann, L. Cooper, D. Menicanin, A. Zannettino, and S. Gronthos. 2014. EZH2 and KDM6A act as an epigenetic switch to regulate mesenchymal stem cell lineage specification. *Stem Cells.* 32:802–815. http://dx.doi.org/10.1002/stem.1573

Hiramuki, Y., T. Sato, Y. Furuta, M.A. Surani, and A. Sehara-Fujisawa. 2015. Mest but not MiR-335 affects skeletal muscle growth and regeneration. *PLoS One.* 10:e0130436. http://dx.doi.org/10.1371/journal.pone.0130436

Huot, M.E., N. Bisson, L. Davidovic, R. Mazroui, Y. Labelle, T. Moss, and E.W. Khandjian. 2005. The RNA-binding protein fragile X-related 1 regulates somite formation in *Xenopus laevis*. *Mol. Biol. Cell.* 16:4350–4361. http://dx.doi.org/10.1091/mbc.E05-04-0304

Le Dour, C., W. Wu, V. Béréziat, J. Capeau, C. Vigouroux, and H.J. Worman. 2017. Extracellular matrix remodeling and transforming growth factor-β signaling abnormalities induced by lamin A/C variants that cause lipodystrophy. *J. Lipid Res.* 58:151–163. http://dx.doi.org/10.1194/jlr.M071381

Lee, S.J., Y.S. Jung, M.H. Yoon, S.M. Kang, A.Y. Oh, J.H. Lee, S.Y. Jun, T.G. Woo, H.Y. Chun, S.K. Kim, et al. 2016. Interruption of progerin-lamin A/C binding ameliorates Hutchinson-Gilford progeria syndrome phenotype. *J. Clin. Invest.* 126:3879–3893. http://dx.doi.org/10.1172/JCI84164

Li, L.C., and R. Dahiya. 2002. *Bioinformatics.* 18:1427–1431. MethPrimer: designing primers for methylation PCRs

Lin, X., L. Wu, Z. Zhang, R. Yang, Q. Guan, X. Hou, and Q. Wu. 2014. MiR-335-5p promotes chondrogenesis in mouse mesenchymal stem cells and is regulated through two positive feedback loops. *J. Bone Miner. Res.* 29:1575–1585. http://dx.doi.org/10.1002/jbmr.2163

Lujambio, A., and S.W. Lowe. 2012. The microcosmos of cancer. *Nature.* 482:347–355. http://dx.doi.org/10.1038/nature10888

Lund, E., A.R. Oldenburg, E. Delbarre, C.T. Freberg, I. Duband-Goulet, R. Eskeland, B. Buendia, and P. Collas. 2013. Lamin A/C-promoter

interactions specify chromatin state-dependent transcription outcomes. *Genome Res.* 23:1580–1589. http://dx.doi.org/10.1101/gr.159400.113

Lund, E.G., I. Duband-Goulet, A. Oldenburg, B. Buendia, and P. Collas. 2015. Distinct features of lamin A-interacting chromatin domains mapped by ChIP-sequencing from sonicated or micrococcal nuclease-digested chromatin. *Nucleus.* 6:30–39. http://dx.doi.org/10.4161/19491034.2014.990855

Lupiáñez, D.G., M. Spielmann, and S. Mundlos. 2016. Breaking TADs: How alterations of chromatin domains result in disease. *Trends Genet.* 32:225–237. http://dx.doi.org/10.1016/j.tig.2016.01.003

Meyer, S.U., S. Sass, N.S. Mueller, S. Krebs, S. Bauersachs, S. Kaiser, H. Blum, C. Thirion, S. Krause, F.J. Theis, and M.W. Pfaffl. 2015. Integrative analysis of microRNA and mRNA data reveals an orchestrated function of microRNAs in skeletal myocyte differentiation in response to TNF-α or IGF1. *PLoS One.* 10:e0135284. http://dx.doi.org/10.1371/journal.pone.0135284

Mikkelsen, T.S., Z. Xu, X. Zhang, L. Wang, J.M. Gimble, E.S. Lander, and E.D. Rosen. 2010. Comparative epigenomic analysis of murine and human adipogenesis. *Cell.* 143:156–169. http://dx.doi.org/10.1016/j.cell.2010.09.006

Miklós, I., and I.M. Meyer. 2005. A linear memory algorithm for Baum-Welch training. *BMC Bioinformatics.* 6:231. http://dx.doi.org/10.1186/1471-2105-6-231

Naetar, N., and R. Foisner. 2009. Lamin complexes in the nuclear interior control progenitor cell proliferation and tissue homeostasis. *Cell Cycle.* 8:1488–1493. http://dx.doi.org/10.4161/cc.8.10.8499

Naetar, N., B. Korbei, S. Kozlov, M.A. Kerenyi, D. Dorner, R. Kral, I. Gotic, P. Fuchs, T.V. Cohen, R. Bittner, et al. 2008. Loss of nucleoplasmic LAP2α–lamin A complexes causes erythroid and epidermal progenitor hyperproliferation. *Nat. Cell Biol.* 10:1341–1348. http://dx.doi.org/10.1038/ncb1793

Oger, F., C. Gheeraert, D. Mogilenko, Y. Benomar, O. Molendi-Coste, E. Bouchaert, S. Caron, D. Dombrowicz, F. Pattou, H. Duez, et al. 2014. Cell-specific dysregulation of microRNA expression in obese white adipose tissue. *J. Clin. Endocrinol. Metab.* 99:2821–2833. http://dx.doi.org/10.1210/jc.2013-4259

Oldenburg, A.R., E. Delbarre, B. Thiede, C. Vigouroux, and P. Collas. 2014. Deregulation of Fragile X-related protein 1 by the lipodystrophic lamin A p.R482W mutation elicits a myogenic gene expression program in preadipocytes. *Hum. Mol. Genet.* 23:1151–1162. http://dx.doi.org/10.1093/hmg/ddt509

Osmanagic-Myers, S., T. Dechat, and R. Foisner. 2015. Lamins at the crossroads of mechanosignaling. *Genes Dev.* 29:225–237. http://dx.doi.org/10.1101/gad.255968.114

Paulsen, J., M. Sekelja, A.R. Oldenburg, A. Barateau, N. Briand, E. Delbarre, A. Shah, A.L. Sørensen, C. Vigouroux, B. Buendia, and P. Collas. 2017. Chrom3D: three-dimensional genome modeling from Hi-C and nuclear lamin-genome contacts. *Genome Biol.* 18:21. http://dx.doi.org/10.1186/s13059-016-1146-2

Perovanovic, J., S. Dell'Orso, V.F. Gnochi, J.K. Jaiswal, V. Sartorelli, C. Vigouroux, K. Mamchaoui, V. Mouly, G. Bonne, and E.P. Hoffman. 2016. Laminopathies disrupt epigenomic developmental programs and cell fate. *Sci. Transl. Med.* 8:335ra58. http://dx.doi.org/10.1126/scitranslmed.aad4991

Png, K.J., M. Yoshida, X.H. Zhang, W. Shu, H. Lee, A. Rimner, T.A. Chan, E. Comen, V.P. Andrade, S.W. Kim, et al. 2011. MicroRNA-335 inhibits tumor reinitiation and is silenced through genetic and epigenetic mechanisms in human breast cancer. *Genes Dev.* 25:226–231. http://dx.doi.org/10.1101/gad.1974211

Rao, S.S., M.H. Huntley, N.C. Durand, E.K. Stamenova, I.D. Bochkov, J.T. Robinson, A.L. Sanborn, I. Machol, A.D. Omer, E.S. Lander, and E.L. Aiden. 2014. A 3D map of the human genome at kilobase resolution reveals principles of chromatin looping. *Cell.* 159:1665–1680. (published erratum appears in *Cell.* 2015. 162:687–688) http://dx.doi.org/10.1016/j.cell.2014.11.021

Robinson, J.T., H. Thorvaldsdóttir, W. Winckler, M. Guttman, E.S. Lander, G. Getz, and J.P. Mesirov. 2011. Integrative genomics viewer. *Nat. Biotechnol.* 29:24–26. http://dx.doi.org/10.1038/nbt.1754

Rønningen, T., A. Shah, A.R. Oldenburg, K. Vekterud, E. Delbarre, J.O. Moskaug, and P. Collas. 2015. Prepatterning of differentiation-driven nuclear lamin A/C-associated chromatin domains by GlcNAcylated histone H2B. *Genome Res.* 25:1825–1835. http://dx.doi.org/10.1101/gr.193748.115

Rosen, E.D., and O.A. MacDougald. 2006. Adipocyte differentiation from the inside out. *Nat. Rev. Mol. Cell Biol.* 7:885–896. http://dx.doi.org/10.1038/nrm2066

Scaffidi, P., and T. Misteli. 2008. Lamin A-dependent misregulation of adult stem cells associated with accelerated ageing. *Nat. Cell Biol.* 10:452–459. http://dx.doi.org/10.1038/ncb1708

Shah, A., A. Oldenburg, and P. Collas. 2014. A hyper-dynamic nature of bivalent promoter states underlies coordinated developmental gene expression modules. *BMC Genomics.* 15:1186. http://dx.doi.org/10.1186/1471-2164-15-1186

Small, E.M., and E.N. Olson. 2011. Pervasive roles of microRNAs in cardiovascular biology. *Nature.* 469:336–342. http://dx.doi.org/10.1038/nature09783

Stierlé, V., J. Couprie, C. Ostlund, I. Krimm, S. Zinn-Justin, P. Hossenlopp, H.J. Worman, J.C. Courvalin, and I. Duband-Goulet. 2003. The carboxyl-terminal region common to lamins A and C contains a DNA binding domain. *Biochemistry.* 42:4819–4828. http://dx.doi.org/10.1021/bi020704g

Sylvius, N., G. Bonne, K. Straatman, T. Reddy, T.W. Gant, and S. Shackleton. 2011. MicroRNA expression profiling in patients with lamin A/C-associated muscular dystrophy. *FASEB J.* 25:3966–3978. http://dx.doi.org/10.1096/fj.11-182915

Tomé, M., P. López-Romero, C. Albo, J.C. Sepúlveda, B. Fernández-Gutiérrez, A. Dopazo, A. Bernad, and M.A. González. 2011. miR-335 orchestrates cell proliferation, migration and differentiation in human mesenchymal stem cells. *Cell Death Differ.* 18:985–995. http://dx.doi.org/10.1038/cdd.2010.167

Tomé, M., J.C. Sepúlveda, M. Delgado, J.A. Andrades, J. Campisi, M.A. González, and A. Bernad. 2014. miR-335 correlates with senescence/aging in human mesenchymal stem cells and inhibits their therapeutic actions through inhibition of AP-1 activity. *Stem Cells.* 32:2229–2244. http://dx.doi.org/10.1002/stem.1699

Vadrot, N., I. Duband-Goulet, E. Cabet, W. Attanda, A. Barateau, P. Vicart, F. Gerbal, N. Briand, C. Vigouroux, A.R. Oldenburg, et al. 2015. The p.R482W substitution in A-type lamins deregulates SREBP1 activity in Dunnigan-type familial partial lipodystrophy. *Hum. Mol. Genet.* 24:2096–2109. http://dx.doi.org/10.1093/hmg/ddu728

van't Padje, S., B. Chaudhry, L.A. Severijnen, H.C. van der Linde, E.J. Mientjes, B.A. Oostra, and R. Willemsen. 2009. Reduction in fragile X related 1 protein causes cardiomyopathy and muscular dystrophy in zebrafish. *J. Exp. Biol.* 212:2564–2570. http://dx.doi.org/10.1242/jeb.032532

Vasudevan, S., Y. Tong, and J.A. Steitz. 2007. Switching from repression to activation: MicroRNAs can up-regulate translation. *Science.* 318:1931–1934. http://dx.doi.org/10.1126/science.1149460

Vigouroux, C., M. Auclair, E. Dubosclard, M. Pouchelet, J. Capeau, J.C. Courvalin, and B. Buendia. 2001. Nuclear envelope disorganization in fibroblasts from lipodystrophic patients with heterozygous R482Q/W mutations in the lamin A/C gene. *J. Cell Sci.* 114:4459–4468.

Vigouroux, C., M. Caron-Debarle, C. Le Dour, J. Magré, and J. Capeau. 2011. Molecular mechanisms of human lipodystrophies: From adipocyte lipid droplet to oxidative stress and lipotoxicity. *Int. J. Biochem. Cell Biol.* 43:862–876. http://dx.doi.org/10.1016/j.biocel.2011.03.002

Wang, L., Q. Jin, J.E. Lee, I.H. Su, and K. Ge. 2010. Histone H3K27 methyltransferase Ezh2 represses *Wnt* genes to facilitate adipogenesis. *Proc. Natl. Acad. Sci. USA.* 107:7317–7322. http://dx.doi.org/10.1073/pnas.1000031107

Yang, D., D. Lutter, I. Burtscher, L. Uetzmann, F.J. Theis, and H. Lickert. 2014. miR-335 promotes mesendodermal lineage segregation and shapes a transcription factor gradient in the endoderm. *Development.* 141:514–525. http://dx.doi.org/10.1242/dev.104232

Yi, S.A., S.H. Um, J. Lee, J.H. Yoo, S.Y. Bang, E.K. Park, M.G. Lee, K.H. Nam, Y.J. Jeon, J.W. Park, et al. 2016. S6K1 phosphorylation of H2B mediates EZH2 trimethylation of H3: A determinant of early adipogenesis. *Mol. Cell.* 62:443–452. http://dx.doi.org/10.1016/j.molcel.2016.03.011

Zhang, Y., C.H. Wong, R.Y. Birnbaum, G. Li, R. Favaro, C.Y. Ngan, J. Lim, E. Tai, H.M. Poh, E. Wong, et al. 2013. Chromatin connectivity maps reveal dynamic promoter-enhancer long-range associations. *Nature.* 504:306–310. http://dx.doi.org/10.1038/nature12716

Zhu, L., L. Chen, C.M. Shi, G.F. Xu, L.L. Xu, L.L. Zhu, X.R. Guo, Y. Ni, Y. Cui, and C. Ji. 2014. MiR-335, an adipogenesis-related microRNA, is involved in adipose tissue inflammation. *Cell Biochem. Biophys.* 68:283–290. http://dx.doi.org/10.1007/s12013-013-9708-3